Quantitative Evaluation of Correction Methods and Simulation of Motion Artifacts for Rotary Pullback Imaging Catheters

Elham Abouei[a,b,*], Anthony M. D. Lee[b], Geoffrey Hohert[b], Pierre Lane[b], Stephen Lam[b], Calum MacAulay[b]

[a]University of British Columbia, Department of Physics and Astronomy, Vancouver, Canada
[b]British Columbia Cancer Research Center, Department of Integrative Oncology, 675 West 10th Avenue, Vancouver, British Columbia, Canada, V5Z 1L3
eabouei@bccrc.ca

Abstract: In this work, we present a quantitative study based on the ground truth image and artificial motion artifacts and its correction using azimuthal *en face* image registration (AEIR) method. Motion artifacts in the *in vivo* imaging make identification of features and structures like blood vessels challenging. Correction of distortions of tissue features resultant from motion artifacts may enhance image quality and interpretation of images. Optical coherence tomography (OCT) and autofluorescence imaging (AFI) has been reported for *in vivo* endoscopic imaging. Motion artifacts in pulmonary OCT-AFI data sets may be estimated from both AFI and OCT images based on azimuthal registration of slowly varying structures in the 2D en face image. In our previous work, we have described a simulation of motion artifacts for 3D or 2D rotational catheter data and AEIR method, correcting motion artifacts. Our simulated artifacts may be applied on a ground truth image to create an image with known artifacts for the quantitative evaluation of performance of the correction methods. Since there might be some non-visible motion artifacts in the original ground truth image, we need apply the correction method before applying the simulated artifacts. However, there is no guarantee that this process converges to a motion-free scan; also the pre-corrected ground truth image is subjected to the correction method for further quantitative analysis. Here, we present a study for quantitative evaluations on a ground truth image of *in silico* phantom, NURD phantom and *in vivo* OCT and AF images.

Keywords: medical and biological imaging, optical coherence tomography, endoscopic imaging, motion estimation and correction, non-uniform rotation distortion

1 Introduction

In vivo imaging is increasingly developed to enhance our understanding of disease. A combined endoscopic optical coherence tomography (OCT) and autofluorescence imaging (AFI) system can produce complementary information which may enable increased detection and characterization of structural and functional features associated with different diseases[(1)]. OCT and AFI systems are often catheter based for *in vivo* clinical imaging where have been developed for cardiology, gastroenterology, and pulmonology[(2),(3),(4),(5),(6)]. Successful application of catheter-based systems for *in vivo* imaging is challenging since motion artifacts associated with the cardiac cycle, breathing, and non-uniform rotation distortion (NURD) degrade image quality that make identification of structures like blood vessels difficult[(5)]. Cardiac and breathing motion artifacts may be reduced to some degree by decreasing the image acquisition time, but even then there remains a need to compensate for NURD artifacts.

Motion compensation may improve image quality and subsequent interpretation. Several techniques have been investigated to correct NURD in catheter-based OCT systems. Structural landmarks or fiducial markers, and Reflections from the sheath or optical components of the catheters have been used to register successive frames for correcting NURD artifacts[(7),(8),(9)]. Another method has measured the rotational speed of a catheter to correct for NURD artifacts by determining the statistical variation in the speckle between adjacent A-lines[(10)]. Other studies have registered adjacent A-lines or frames by maximizing the cross correlation between the speckle in adjacent search regions[(5),(11)]. However, poor tissue apposition regions can result in inaccurate rotational speed interpolation and methods using cross correlation or phase information may be more sensitive to speckle noise, and generally require highly correlated A-line data. We have presented a new method called azimuthal *en face* image registration (AEIR), and it is applicable to any 2D or 3D rotational catheter data.

In order to quantitatively evaluate the correction methods, previously we have developed a metric by applying simulated motion artifacts in *in vivo* images. These artificial artifacts may be applied on a ground truth image to create an image with known artifacts. Since there might be some non-visible motion artifacts, we need to apply correction method before applying the simulated artifacts. However, there is no guarantee that this process converges to a motion-free scan. It is more likely that the corrected image is distorted dependant on the alignment algorithm. From this stable point, it is expected that the same algorithm, based on the same data, is more likely to return to its previous stable state. The other correction methods, for whom different stable state are expected, would have a non-optimal error metric even if no motion artifact is applied, which puts them at a disadvantage.

In this work, we are studying the ground truth image used for the quantitative analysis and tendency of different correction methods on ground truth image on the quantitative metric. We present quantitative evaluations performed on ground truth images of an *in*

silico phantom, a NURD phantom and *in vivo* endoscopic pulmonary OCT and AF datasets of peripheral lung airways, and applied simulated artifacts.

2 Materials and Methods

2.1 Phantom and *In Vivo* Imaging

A combined endoscopic OCT-AFI instrument using a double-clad fiber (DCF) catheter was used in this study to collect OCT and AFI signals simultaneously and custom data acquisition software collects and processes the data for immediate display. The OCT subsystem employs a 50.4 kHz wavelength-swept source (SSOCT-1310, Axsun Technologies Inc., Billerica, MA, USA) with the illumination centered at 1310 nm with 100 nm bandwidth. The AFI subsystem uses a 445 nm semiconductor laser (CUBE 445-40C, Coherent, Santa Clara, CA, USA). A rotary-pullback drive unit allows 3D OCT-AFI imaging of airways up to 7 cm in length.(1)

OCT and AF imaging of a NURD phantom and human subjects were collected. The NURD phantom was a 3D-printed object containing eight evenly-spaced parallel features oriented along the pullback direction. It quantifies NURD artifacts during imaging as deviations from the expected geometry.(12) *In vivo* pulmonary imaging of human subjects was performed during flexible bronchoscopy. It was approved by the Research Ethics Board of the University of British Columbia and the British Columbia Cancer Agency.

2.1 Motion Artifacts Correction Method

The motion correction method called AEIR was described in our previous work(13). Here, we briefly describe it. Our motion artifact correction method is based on calculating the correlation between pixels along the rotational direction and the corresponding adjacent pixels in the pullback direction from a previous frame. Continuous angular mismatch corresponding to motion artifacts can be estimated by assuming that slowly varying structures exist in the direction of the pullback in the *en face* image. These structures arise from biological features, such as the alveoli, collagen network, and vascular networks.

The 2D mean-intensity projection of OCT volume or 2D AFI is presented as an *en face* image $I(p,f)$, where p is the rotation index position in pixels and f is the frame index. In order to reduce speckle noise, the $I(p,f)$ calculated from OCT image is smoothed using a 3x3 pixel median filter. Then strips of length ($W=2w+1$)-pixels are centered on each pixel along the rotational direction on the $I(p,f)$ image (the strips reach the temporally closest pixels from neighboring image's frame at the beginning and end of each frame). A cost matrix using Eq.1 is constructed to compare each strip $S_{p,f+1}(W)$ from the $(f+1)^{th}$ frame to $(2n+1)$ strips from the previous pullback frame f, ($S_{p-n,f}(W)$, $S_{p+n,f}(W)$). In this notation, p represents the p^{th} pixel/strip in the frame and n determines the number of strips in the f^{th} frame.

$$Cost_{f+1}(k,p) = \left(\sum_W (S_{p+k,f}(W) - S_{p,f+1}(W))^2\right)^2 \quad \text{Eq.1}$$

where $Cost_{f+1}(k,p)$ is the value of the cost matrix at its k^{th} row and p^{th} column between frame f and $f+1$ with $k \in [-n,n]$. In order to maintain the continuity of frames, $Cost_{f+2}(k,p)$ is concatenated to $Cost_{f+1}(k,p)$. The concatenated matrix, *Cost(k,P)*, with $P \in [1,2 \times p]$ is resampled by stretching the vertical *k*-direction with a parameter named *s* and downsampled along *P*-direction with a parameter named *m*. An optimal continuous path (OCP) through the cost matrix using dynamic programming (DP) is found. The OCP represents the continuous rotation of the catheter and accounts for motion artifacts. Thereafter, the OCP is resampled to its original size. Image correction can be applied by reversing the obtained OCP [14]. The same correction is applied to the 3D frames as each pixel in the *I(p,f)*-frame representing its corresponding A-line in the 3D frame. Since the OCT and AF images were obtained simultaneously, we could use corrections from either the *en face* OCT image or AFI, denoted as $AEIR_{meanProj}$ and $AEIR_{AF}$, respectively. (Images were processed in MATLAB R2016a; interpolation methods were specified to use "bicubic" for resizing image and "Pchip" for aligning pixels or A-lines.) We have applied the correction parameters for our AEIR methods on our datasets that were found to be optimal (w=20, n=20, s=5, and m=1[13]).

Azimuthal registration of image sequences (ARIS) used DP for correction of NURD artifacts in OCT images, where L2 norm was used to calculate the cost matrix from full A-lines of OCT frames[11]. We have compared corrections based on full A-lines in the OCT frame where the cost matrix calculated using the Eq.1 with our correction method based on the W-pixel strip in the *en face* image. In order to achieve the best results for $ARIS_{OCT}$ method (), the OCT data was smoothed using a 3x3 pixels median filter for intraframe filtering (along the A-line and azimuthal direction on each frame) and a mean filter of size 5 frames for interframe averaging. The $ARIS_{OCT}$ method using the same n, s, and m parameters as AEIR method was applied on the OCT images.

2.2. Motion Artifacts Simulation for *In Vivo* Rotary Pullback Catheter

Quantitative evaluation for a motion correction method requires a priori knowledge of the artifacts in the image to compare against the applied correction. We simulated motion artifacts in endoscopic OCT and AF images, and described it in our previous work[13]. Here, we briefly describe our model, which was constructed of sinusoidal patterns with different frequencies along the pullback direction in our NURD phantom and *in vivo* images data sets. [7],[10], [12], [15] *In vivo* biological artifact frequencies are ~0.2Hz and 1-2 Hz for breathing and heart beat based artifacts, respectively, whereas non-biological NURD artifact frequencies can be lower and/or higher. The motion artifacts were simulated as a combination of wavelets (Eq.2) particular to each type of artifact along the pullback direction.

$$A_i(f) = a_i \sin(freq_i \,.\, f) \,.\, e^{\frac{-(f-f_{0,i})^2}{\sigma_i}} \quad \text{Eq.2}$$

where $A_i(f)$ is simulated artifact, a_i is the amplitude of the artifact, $freq_i$ is the frequency of the artifact, f is the position (frame) of the wavelet along the pullback direction, $f_{0,i}$ is the position of artifacts centered along the pullback, and σ_i is the artifacts' length along pullback direction. An artifact matrix *A(p,f)*, the same size as the *I(p,f)*, is generated where each $A_i(f)$ displaces pixel (p_i) along the rotation direction. The other pixels in between these displaced pixels are interpolated considering wrapping of each frame to its next frame. The *A(p,f)* matrix is output of our motion artifacts simulation was applied to ground truth images of NURD phantom and *in vivo* image to generate ground truth images with known artifacts.

2.3 Quantitative Evaluation of Motion Correction

We have selected three pullbacks, one with no motion artifacts from an *in silico* phantom, and two pullbacks with only minor visible motion artifacts from NURD phantom and *in vivo* image. Afterwards, we iteratively applied a correction method on the NURD phantom and *in vivo* images to correct for unobservable artifacts that are detectable by the method until there was little change between corrections. We have iteratively applied $AIER_{AF}$ and $AEIR_{meanProj}$ correction methods in order to generate two separate pre-corrected ground truth images. The artificial artifacts were added to these pre-corrected ground truth images, and then corrected using three correction methods.

Each correction method results in a correction matrix (C) representing the artifacts detected in the image to be corrected. The correlation coefficient (r) and average compensated difference ($\overline{D}_{comp}$) were designed for quantitative evaluation of the correction methods, where $\overline{D}_{comp}$ is calculated by Eq.3 and Eq.4[13]. Results with a high r value and a low $\overline{D}_{comp}$ value define better motion correction.

$$D_{comp}(f,p) = D(f,p) - D(f-1,p)\,,\ \ f \geq 2\ and\ D_{comp}(1,p) = D(1,p) \quad \text{Eq. 3}$$

$$\overline{D}_{comp} = \overline{|D_{comp}(f,p)|} \quad \text{Eq. 4}$$

Where *D(f,p)* is difference between C and A matrices.

Since there might be some non-visible motion artifacts in the NURD phantom and *in vivo* OCT-AF images, we need to apply correction method before applying the simulated artifacts and subsequent quantitative analysis. We have previously applied AEIR_AF on the ground truth images for quantitative analysis. However, there is no guarantee that this process converges to a motion-free ground truth images. It is more likely that the corrected image is distorted dependant on the alignment algorithm. However, from this stable point, it is expected that the same algorithm, based on the same data, is more likely to return to its previous stable state. The other correction methods, for which a different stable state is expected, would have a non-optimal error metric even if no motion artifact is applied, which puts them at a disadvantage. Here, we have studied the effect of pre-correction on the ground truth image by applying $AEIR_{AF}$ and $AEIR_{meanProj}$ on the ground

truth image. Then, we may evaluate the performance of quantitative metrics, r and $\overline{D}_{comp}$, for comparing different correction methods.

3 Results and Discussions

We have visually evaluated the correction methods on *en face* images. NURD artifacts were corrected by reducing its oscillation frequency and cardiac and breathing artifacts by reducing the high amplitude low frequency oscillations. In order to quantify correction methods, we have used a quantitative method that was proposed in our previous work[13]. In this work, we are studying the ground truth image used for the quantitative analysis and tendency of different correction methods on ground truth image in the quantitative metric.

We have simulated eight models of motion artifacts for *in vivo* rotary-pullback catheter imaging (Fig. 1). Figure 1.a1-4 show four examples for cardiac and NURD artifacts and Fig 1.a5-8 show four examples for cardiac and NURD, as well as breathing artifacts. These simulated artifacts are added to a ground truth image, which is expected to have no intrinsic motion artifacts. Figures 1.b-c are provided for the quantitative evaluation of the three correction methods on an *in silico* phantom where there is no intrinsic motion artifacts in the ground truth image.

Quantitative evaluation of the three correction methods were performed on one image from a NURD phantom and one *in vivo* endoscopic pulmonary OCT and AF dataset from a peripheral lung airway with eight simulated artifacts where the starting ground truth images likely have minor non-visible motion artifacts. We have iteratively applied the $AEIR_{AF}$ and $AEIR_{meanProj}$ methods on each ground truth image to study the effect of pre-correction method on the ground truth image for when comparing the final results. Figure 2 and 3 show results of the quantitative analysis on the NURD phantom and the *in vivo* image, respectively. In Fig. 2 and 3, (a) and (d) are showing the r and $\overline{D}_{comp}$metrics on the original image with no pre-correction, (b) and (e) showing r and $\overline{D}_{comp}$ on the pre-corrected image with $AEIR_{AF}$, and (c) and (f) showing r and $\overline{D}_{comp}$ on the pre-corrected image with $AEIR_{meanProj}$. As it can be seen from these figures, results for both pre-correction methods $AEIR_{AF}$ and $AEIR_{meanProj}$ are similar regarding the performance of each method for correcting motion artifacts. However, the use of no pre-correction method on the original image results in a poor estimation artifact reduction when comparing the performance of the three methods. In addition, comparing the results from the *in silico* phantom (Fig. 1.b-c) with the NURD phantom and *in vivo* images, it could be concluded that we need to apply a pre-correction method on the original image to be used as the ground truth image before applying the simulated motion artifacts. So to evaluate the performance of the different algorithms there is a need for a preprocessing of the ground truth image to reduce motion artifacts within the ground truth image to remove minor non-visible motion artifacts prior to the rest of the evaluation process. The simulated motion artifacts are added to the pre-corrected ground truth image for quantitative evaluation of correction methods.

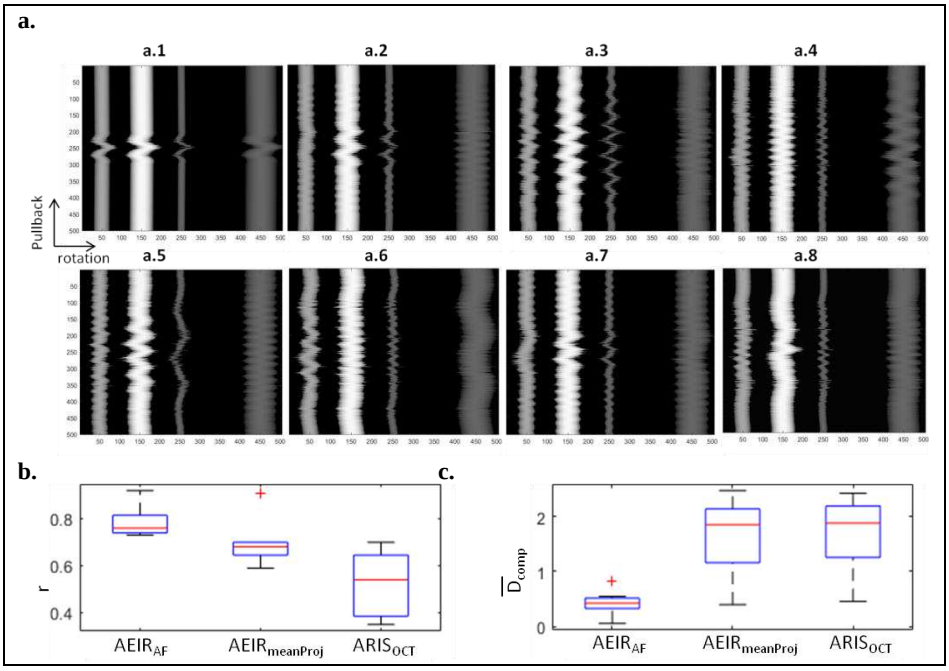

Fig 1. Simulation of motion artifacts. (a) Eight simulated artifacts on the *in silico* phantom, (b) and (c) are r and $\bar{D}_{comp}$ comparison on the *in silico* phantom, respectively.

Analyses of motion corrections on the NURD phantom and *in vivo* images with the artificial artifacts in Fig. 1.a were done using the two metrics. As it can be seen in Fig. 2-3, for the $ARIS_{OCT}$ method, it is not sufficient to compare full A-lines for motion correction since there is a reduced or absent feature correlation between A-lines in the data. However, motion correction with our AEIR method appears effective since each strip is mean projection of W number of A-lines that were compared to each other.

We also considered the run-time which is the average time required to apply the correction to all frames of one image. The average run-time to apply the correction per frame was 0.10, 0.10, and 0.25 s for $AEIR_{AF}$, $AEIR_{meanProj}$, and $ARIS_{OCT}$, respectively. In addition, AEIR method calculated the correction of motion artifacts about 2-3 times computationally faster than the OCT-$ARIS_{OCT}$ by using the *en face* image for correction rather than its full 3D stack/OCT-volume.

In summary, we need to apply a pre-correction method to the original image to be used as the ground truth image before applying the simulated motion artifacts for quantitative evaluation of the various correction methods. Motion correction may be achieved by either AEIRmeanProj or AEIRAF on *in vivo* images with our AEIR method. The AEIR method allows for correction of motion artifacts along the rotational direction in rotary-pullback 2D and 3D image modalities. It corrects images along the rotational direction using the mean projection of A-lines from *en face* image, which improves correction compared to using the full A-lines data. The performance of $AEIR_{AF}$ method is enhanced compared to the $AEIR_{meanProj}$ method for images that have strong AF signal because of good contrast structures in the image. It is considerable that the two methods may be complementary methods when both modalities are simultaneously obtained to combine the effectiveness of each in different parts of the pullback. In addition, the r and $\overline{D}_{comp}$ metrics may be used to quantitatively evaluate the correction methods. These quantitative analyses on more real data seem necessary for a more complete body of work.

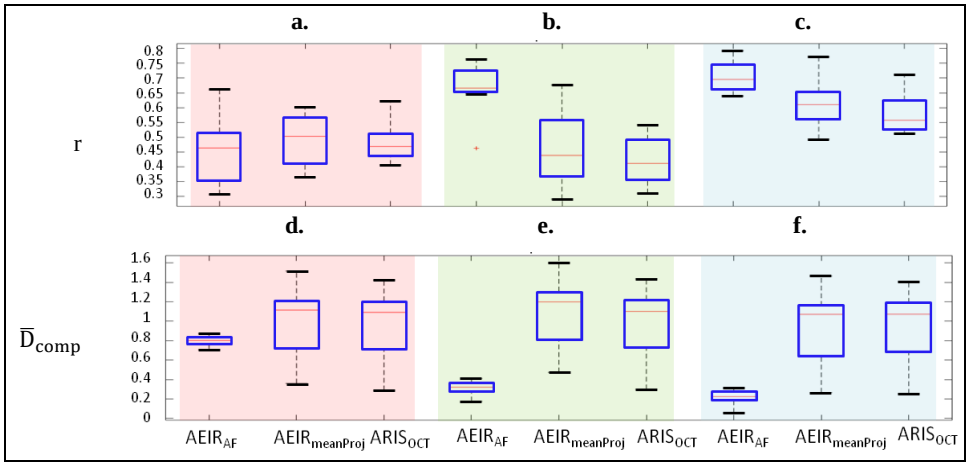

Fig 2. Quantitative analysis of three correction methods on a NURD phantom.(a) and (d) are original ground truth image, (b) and (e) are $AEIR_{AF}$ pre-corrected ground truth image, and (c) and (f) are $AEIR_{meanProj}$ pre-corrected ground truth image.

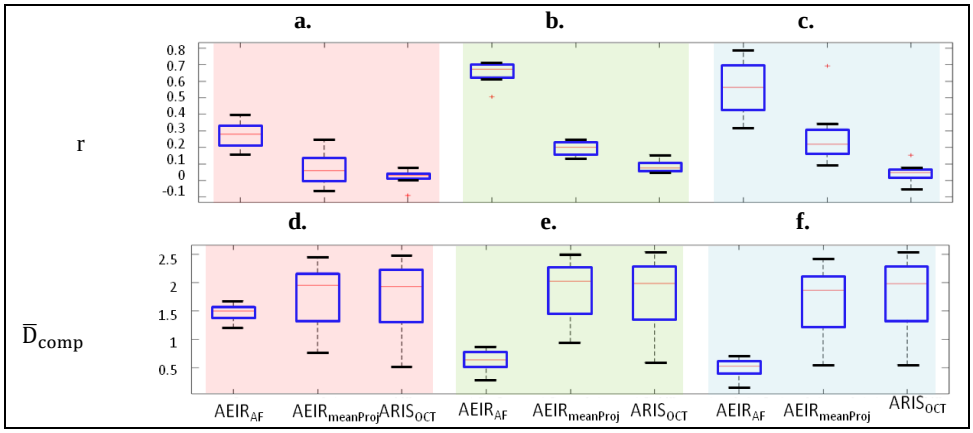

Fig 3. Quantitative analysis of three correction methods on a *in vivo* image.(a) and (d) are original ground truth image, (b) and (e) are $AEIR_{AF}$ pre-corrected ground truth image, and (c) and (f) are $AEIR_{meanProj}$ pre-corrected ground truth image.

Acknowledgment

This work was supported by Canadian institutes of health research (CIHR) (ppp-141717).

References

1. Pahlevaninezhad H. *et al.*, "Endoscopic Doppler optical coherence tomography and autofluorescence imaging of peripheral pulmonary nodules and vasculature.", *Biomedical optics express*, **6(10)**, 4191–9, (2015).
2. Yonetsu T. *et al.*, "Optical Coherence Tomography- 15 Years in Cardiology", *Circulation Journal*, **77(August)**, 1933–1940, (2013).
3. Pahlevaninezhad H. *et al.*, "Multimodal tissue imaging: using coregistered optical tomography data to estimate tissue autofluorescence intensity change due to scattering and absorption by neoplastic epithelial cells", *Journal of Biomedical Optics*, **18(10)**, 106007, (2013).
4. Evans J. A. *et al.*, "Identifying intestinal metaplasia at the squamocolumnar junction by using optical coherence tomography", *Gastrointest Endosc*, **65(1)**, 50–56, (2007).
5. Kang W. *et al.*, "Motion artifacts associated with in vivo endoscopic OCT images of the esophagus.", *Optics express*, **19(21)**, (2011).
6. Pahlevaninezhad H. *et al.*, "Endoscopic high-resolution autofluorescence imaging and OCT of pulmonary vascular networks", *Optics letters*, **41(14)**, 3209–3212, (2016).
7. Ahsen O. O. *et al.*, "Correction of rotational distortion for catheter-based en face OCT and OCT angiography.", *Optics letters*, **39(20)**, 5973–6, (2014).
8. Ughi G. J. *et al.*, "Automatic three-dimensional registration of intravascular optical coherence tomography images.", *Journal of biomedical optics*, **17(2)**, 26005, (2012).
9. Sun C. *et al.*, "In vivo feasibility of endovascular Doppler optical coherence tomography", *Biomedical optics express*, **3(10)**, 2600–2610, (2012).

10. Uribe-Patarroyo Né. *et al.*, "Rotational distortion correction in endoscopic optical coherence tomography based on speckle decorrelation", *Optics letters*, **40(23)**, 5518–5521, (2015).
11. Soest G. van *et al.*, "Azimuthal Registration of Image Sequences Affected by Nonuniform Rotation Distortion", *IEEE Transactions on Information Technology in Biomedicine*, **12(3)**, 348–355, (2008).
12. Hohert G. *et al.*, "3D-printed phantom for the characterization of non-uniform rotational distortion (Conference Presentation)", *Proc SPIE, Design and Quality for Biomedical Technologies IX*, **9700**, (2016).
13. Abouei E. *et al.*, "Correction of motion artifacts in endoscopic optical coherence tomography and autofluorescence images based on azimuthal en face image registration", *Journal of biomedical optics*, **23(1)**, (2018).
14. Cua M. *et al.*, "Lung vasculature imaging using speckle variance optical coherence tomography", *Proc of SPIE*, **8207**, 82073P–82073P–7, (2012).
15. Kang W. *et al.*, "Motion artifacts associated with in vivo endoscopic OCT images of the esophagus.", *Optics express*, **19(21)**, (2011).